


## Quantum Enhanced Precision Estimation of Transmission with Bright Squeezed Light

G.S. Atkinson<sup>1,2,\*</sup> E.J. Allen,<sup>1</sup> G. Ferranti,<sup>1</sup> A.R. McMillan,<sup>1</sup> and J.C.F. Matthews<sup>1,†</sup>

<sup>1</sup>*Quantum Engineering Technology Labs, H. H. Wills Physics Laboratory and Department of Electrical & Electronic Engineering, University of Bristol, Tyndall Avenue, Bristol BS8 1FD, United Kingdom*

<sup>2</sup>*Quantum Engineering Centre for Doctoral Training, H. H. Wills Physics Laboratory and Department of Electrical & Electronic Engineering, University of Bristol, Tyndall Avenue, Bristol BS8 1FD, United Kingdom*

 (Received 24 February 2021; revised 24 August 2021; accepted 3 September 2021; published 19 October 2021)

Squeezed light enables measurements with sensitivity beyond the quantum noise limit (QNL) for optical techniques such as spectroscopy, gravitational wave detection, magnetometry, and imaging. Precision of a measurement—as quantified by the variance of repeated estimates—has also been enhanced beyond the QNL using squeezed light. However, sub-QNL sensitivity is not sufficient to achieve sub-QNL precision. Furthermore, demonstrations of sub-QNL precision in estimating transmission have been limited to picowatts of probe power. Here we demonstrate simultaneous enhancement of precision and sensitivity to beyond the QNL for estimating modulated transmission with a squeezed amplitude probe of 0.2 mW average (25 W peak) power, which is 8 orders of magnitude above the power limitations of previous sub-QNL precision measurements of transmission. Our approach enables measurements that compete with the optical powers of current classical techniques, but have both improved precision and sensitivity beyond the classical limit.

DOI: [10.1103/PhysRevApplied.16.044031](https://doi.org/10.1103/PhysRevApplied.16.044031)

### I. INTRODUCTION

Optical measurements are fundamentally limited by quantum fluctuations in the probe. The Poisson-distributed photon number  $n$  of coherent light—often used as a probe in classical experiments—results in shot noise, which represents the quantum noise limit (QNL) in the precision of parameter estimation with classical resources [1]. Because the QNL scales with  $\sim 1/\sqrt{n}$ , longer measurements and higher intensity can increase precision. One may also increase precision with more interaction between probe and sample via multiple passes [2,3] or optimizing sample length [4]. However, there can often be restrictions on the total optical exposure, the measurement time, and sample properties [5]. By using nonclassical light, the fluctuations in the probe can be reduced below the QNL, thus providing “sub-shot-noise” precision per photon [6]. The QNL defines the best precision achievable without the use of quantum correlations for a given apparatus and average photon number [7]. This is distinguished from the standard quantum limit, which defines a measurement-independent limit to the precision that may be achieved using a minimum uncertainty state of a given average photon number, without quantum resources [8]. Because squeezed light can

offer significant reduction in noise below the QNL [9], and can be generated with arbitrary intensity using coherent laser light [10], it offers a practical approach for enhancing optical techniques beyond classical limitations.

Precision in measuring a parameter can be quantified by the inverse of the variance of corresponding measurement outcomes, and is bounded by the Fisher information according to the Cramér-Rao bound [11]. By contrast, the sensitivity of a measurement is the smallest possible signal that may be observed [12], and thus depends only on the signal-to-noise ratio (SNR). Photonic (definite photon number) quantum metrology uses photon counting to observe quantum correlations between modes to reduce the noise of a measurement [13–15]. Here one can attain an improvement in both precision and sensitivity, by increasing the Fisher information and reducing the optical noise floor. However, due to limitations in both the maximum photon flux and detector saturation power, the probe powers achievable are in practice  $\mathcal{O}(10^6)$  photons detected per second (pW) [13,14], which limits use to only cases that are reliant on ultralow intensities. Homodyne detection of squeezed vacuum has been used to estimate phase with sub-QNL precision [16,17]. This is possible because measurement is performed away from low-frequency technical noise, in a shot-noise-limited bandwidth where squeezing reduces vacuum noise. However, as with photonic quantum metrology, strategies using squeezed vacuum for

\*ga12779@my.bristol.ac.uk

†jonathan.matthews@bristol.ac.uk

sub-QNL precision have also been restricted in maximum optical probe power.

Measurements using high-power squeezed light can reach sub-QNL sensitivity in detection of phase modulation [6] and amplitude modulation (AM) [18]. This is because modulation introduces ac components in the detected signal, which can be made to coincide with a shot-noise-limited detector bandwidth, while squeezed light reduces the optical noise relative to the signal. The sensitivity of any frequency-domain measurement of an optical signal in a shot-noise-limited bandwidth may be improved by such techniques and this has been demonstrated in a range of applications (e.g., [7,19–30]). However, enhancing sensitivity is not a sufficient condition to enhance precision. When bright optical probes are used, the noise in the bright field often dominates over the vacuum noise, which prohibits the use of squeezed light for reaching precision beyond the QNL. For squeezed light to provide a precision improvement in such a measurement, the variance of the measured signal must be limited by optical shot noise. Here, we fulfill this condition and use bright-amplitude squeezed light to measure modulated transmission with precision beyond the QNL.

## II. THEORY

The parameter estimated in this work is the modulation index  $\delta_m = (P - P')/P$ , where  $P$  and  $P'$  are the maximum and minimum output power transmitted through a modulated loss [Fig. 1(e)] [1]. For modulation frequency  $\Omega$ , sinusoidal AM generates optical sidebands at  $\pm\Omega$  from the carrier frequency. Upon photodetection, this leads to a single electronic sideband in the spectral noise power at frequency  $\Omega$  that contains information about  $\delta_m$ . Figures 1(a)–1(c) illustrate the behavior of the spectral noise power of an initial laser input [Fig. 1(a)], where the noise characteristics at  $\Omega$  approximate that of a coherent state  $|\alpha\rangle$  and so quantum noise dominates the variance of intensity. The light is subsequently squeezed in amplitude [Fig. 1(b)] and then modulated in amplitude [Fig. 1(c)]. The insets illustrate the ideal evolution of the state at  $\pm\Omega$  for an initial coherent state  $|\alpha\rangle$ . The final state is amplitude squeezed with an average photon number of  $\langle\hat{n}(\pm\Omega)\rangle = \delta_m|\alpha|^2/2$ .

We derive an estimator for  $\delta_m$  from the SNR of direct photodetection, similar to [18] that uses homodyne detection. For direct photodetection of AM in a shot-noise-limited bandwidth around  $\Omega$ , the SNR is given by  $\delta_{\text{SNR}} = \langle p_s \rangle / \langle p_n \rangle$ , where  $\langle p_s \rangle$  is the average signal component of the generated electronic power at  $\Omega$  and  $\langle p_n \rangle$  is the average electronic power generated from optical noise. In the limit of weak AM ( $\delta_m \ll 1$ ), loss due to AM has a negligible effect on the squeezing parameter  $\Phi$  and the average optical power on the modulator output. Therefore, average measured photocurrent is expressed as  $i_0 = q\eta P[1 - (\delta_m/2)]/\hbar\omega \approx q\eta P/\hbar\omega$ , with

electron charge  $q$ , photodiode efficiency  $\eta$ , reduced Planck constant  $\hbar$ , and carrier angular frequency  $\omega$ . We then obtain (see Appendix A)

$$\delta_{\text{SNR}} = \frac{\langle p_s \rangle}{\langle p_n \rangle} \approx \frac{\delta_m^2 i_0}{4q\Phi B}, \quad (1)$$

where  $B$  is the frequency resolution bandwidth (RBW) of the noise spectrum, and corresponds to the inverse of the integration time over which the spectrum is measured. From Eq. (1), we define the estimator

$$\hat{\delta}_m = \sqrt{\frac{4q\Phi B \hat{\delta}_{\text{SNR}}}{i_0}}, \quad (2)$$

where

$$\hat{\delta}_{\text{SNR}} = \frac{p_\Omega - p_N}{p_N - p_E} \text{ and } i_0 = \frac{q\eta\langle P \rangle}{\hbar\omega}. \quad (3)$$

$p_\Omega$ ,  $p_N$ , and  $p_E$  are the spectral noise powers of the electronic sideband, the optical noise floor, and the electronic noise floor, respectively.  $\langle P \rangle$  is the average optical power output from the modulator, and both  $\langle P \rangle$  and  $p_N$  may be precalibrated with high precision. The dependence of  $\hat{\delta}_m$  on the optical noise is then contained in the measurement of  $p_\Omega$ .

For an input resistance of  $R$  to the measuring device (e.g., spectrum analyzer or oscilloscope), we can define the power of the electronic sideband as

$$p_\Omega = 2R|\hat{i}_\Omega|^2, \quad (4)$$

where  $\hat{i}_\Omega$  is the photocurrent in the frequency bin centered on  $\Omega$ . By considering power fluctuations due to quantum optical noise, low-frequency classical optical noise, and electronic noise, we find

$$\begin{aligned} \text{Var}(p_\Omega) &= \langle p_\Omega^2 \rangle - \langle p_\Omega \rangle^2 \\ &\approx \frac{R^2}{M} \left[ 2q\delta_m^2 i_0^3 \Phi B + 4\delta_m^4 i_0^4 \text{Var}(\text{Re}[\mathcal{H}]) \right. \\ &\quad \left. + 4q^2 \delta_m^2 i_0^2 \text{Var}(\text{Re}[\mathcal{N}]) \right] \end{aligned} \quad (5)$$

(see Appendix B).  $\text{Re}[\bullet]$  corresponds to the real part,  $\mathcal{H}$  is the dc component of the classical relative amplitude noise from the laser,  $\mathcal{N}$  is the component of electronic noise in the  $\pm B/2$  frequency interval around  $\Omega$ , and  $M$  is a variance reduction factor due to spectral averaging. The dependence of  $\text{Var}(p_\Omega)$  on  $\mathcal{H}$  is due to classical noise being transferred from the carrier to the optical sidebands upon modulation. We assume here that the variance of the optical noise due to the classical intensity fluctuations scales quadratically with

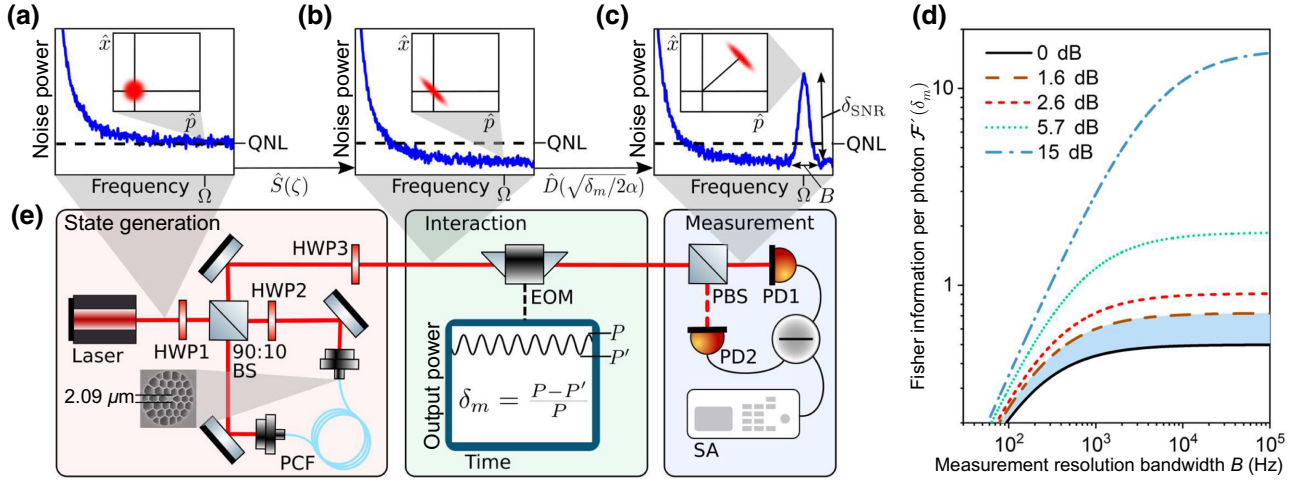


FIG. 1. Modeling enhanced precision measurement of  $\delta_m$ , and experimental setup. (a)–(c) Plots of spectral noise power illustrating the effect of amplitude squeezing and modulation on a typical laser source, with the quadrature diagrams showing a coherent state defined by  $\hat{x}$ ,  $\hat{p}$  at  $\pm\Omega$ . (d) Theoretical model of the Fisher information per detected photon  $\mathcal{F}'(\delta_m)$  for typical laser light that is quantum noise limited at  $\Omega$  (solid line) and squeezed light (dashed lines):  $-1.6$  and  $-2.6$  dB are the measured and inferred generated squeezing levels in our experiment,  $-5.7$  dB is amplitude squeezing previously achieved using an asymmetric Kerr interferometer [31], and  $-15$  dB is the highest measured squeezing to date [9]. For each plot,  $M = 1$ ,  $P = 0.2$  mW,  $\lambda = 740$  nm,  $\eta = 1$ ,  $\delta_m = 1 \times 10^{-4}$  and  $\text{Var}(\text{Re}[\mathcal{H}]) = 1 \times 10^{-5}$ . (e) Schematic of the experiment and SEM image representative of the birefringent photonic crystal fiber (PCF) structure. A pulsed laser at 740 nm propagates into a Sagnac interferometer for squeezed state generation. A PCF provides the nonlinear medium for Kerr squeezing. An electro-optic modulator (EOM) combined with polarizing beam splitter (PBS) are used to generate AM, which is measured with a spectrum analyzer (SA).

optical power, as expected for technical laser noise [32]. To quantify any enhancement in precision obtained by using squeezed light, we compute the classical Fisher information on  $\delta_m$ ,  $\mathcal{F}(\delta_m)$ . Since we use an amplitude squeezed state to perform an amplitude measurement, the classical Fisher information saturates the quantum Cramér-Rao bound [33]—therefore evaluating  $\mathcal{F}(\delta_m)$  bounds any quantum strategy. For our measurement strategy, and assuming  $\alpha \gg 1$ ,  $\hat{\delta}_{\text{SNR}}$  is normally distributed and we can define  $\mathcal{F}(\delta_{\text{SNR}})$  according to [34]

$$\mathcal{F}(\delta_{\text{SNR}}) = \frac{1}{\text{Var}(\hat{\delta}_{\text{SNR}})} = \left[ \left( \frac{\partial \langle \hat{\delta}_{\text{SNR}} \rangle}{\partial \langle p_\Omega \rangle} \right)^2 \text{Var}(p_\Omega) \right]^{-1}. \quad (6)$$

$\mathcal{F}(\delta_m)$  can be obtained from  $\mathcal{F}(\delta_{\text{SNR}})$  by using [34]

$$\mathcal{F}(\delta_m) = \left( \frac{\partial \delta_{\text{SNR}}}{\partial \delta_m} \right)^2 \mathcal{F}(\delta_{\text{SNR}}). \quad (7)$$

We find that  $\text{Var}(\text{Re}[\mathcal{N}])$  contributes negligibly to  $\mathcal{F}(\delta_m)$ , and from Eqs. (2)–(7), this leads to

$$\mathcal{F}(\delta_m) \approx M \left[ \frac{2q\Phi B}{i_0} + 4\delta_m^2 \text{Var}(\text{Re}[\mathcal{H}]) \right]^{-1}. \quad (8)$$

The quantum precision enhancement is then given by the ratio  $\mathcal{Q}(\delta_m)$  between the values of  $\mathcal{F}(\delta_m)$  for squeezed

( $\Phi < 1$ ) and coherent ( $\Phi = 1$ ) light. The variance of  $\hat{\delta}_m$  can be obtained by standard error propagation. We find

$$\text{Var}(\hat{\delta}_m) = \left( \frac{\partial \langle \hat{\delta}_m \rangle}{\partial \langle p_\Omega \rangle} \right)^2 \text{Var}(p_\Omega) = \frac{1}{\mathcal{F}(\delta_m)}. \quad (9)$$

Therefore,  $\hat{\delta}_m$  is an efficient estimator. We also find that, in the limit of weak AM,  $\langle \hat{\delta}_m \rangle = \delta_m$ , meaning our estimator is unbiased.

The Fisher information per detected photon may be defined as  $\mathcal{F}'(\delta_m) = \mathcal{F}(\delta_m)/\langle N \rangle$ , where  $\langle N \rangle = i_0/qB$  is the number of photons detected in the measurement time  $B^{-1}$ . Figure 1(d) illustrates the dependence of  $\mathcal{F}'(\delta_m)$  on the RBW for a typical laser source that is quantum noise limited at  $\Omega$  (solid black line) and various levels of squeezing (dashed lines), with all other parameters fixed. We find that for higher RBWs, squeezing provides sub-QNL precision in estimating  $\delta_m$ . This can be seen from Eq. (8), since for  $2q\Phi B/i_0 \gg 4\delta_m^2 \text{Var}(\text{Re}[\mathcal{H}])$ , quantum noise limits the precision of the measurement, and we find  $\mathcal{Q}(\delta_m) \rightarrow \mathcal{Q}_{\text{opt}}$ , where

$$\mathcal{Q}_{\text{opt}} = \frac{1}{\Phi}. \quad (10)$$

Because all information on  $\delta_m$  is contained at the modulation frequency  $\Omega$ , this model suggests a practically

achievable precision improvement per detected photon by applying amplitude squeezing. In general, this model suggests that, for measurements where the optical signal contains a small fraction  $\delta_m$  of the total measured power, the effect of excess classical noise on precision can be minimized by reducing the integration time  $B^{-1}$  until the measurement saturates the quantum noise limit.

### III. EXPERIMENTAL DETAILS

For the measurement, we built a source of amplitude squeezed light, based on [35]. A Spectra Physics Mai Tai Ti:sapphire laser provides 100-fs pulses with central wavelength  $\lambda_0 = 740$  nm and a peak power of 60 W, which corresponds to 0.5 mW of average power. This light is coupled into an asymmetric Sagnac interferometer, with a 90:10 splitting ratio beam splitter (BS) [Fig. 1(e)]. A 14-m custom-made photonic crystal fiber (PCF), with a core size of 2.09  $\mu\text{m}$ , provides a strong  $\chi^{(3)}$  nonlinearity in the interferometer. The attenuation coefficient of the PCF is 0.1 dB/m. A 14-m length was determined to provide the optimal nonlinear response for the chosen operating laser power level, which was constrained by the saturation limit of the detector. The fiber samples used were originally fabricated for photon pair generation work [36]. As the brighter 90% reflected pulses propagate through the PCF, they undergo self-phase modulation and become quadrature squeezed [10,35]. These pulses interfere with the weaker (10%) counterpropagating pulses transmitted initially at the BS—these provide a coherent displacement in phase space. This leads to amplitude squeezing on the output of the interferometer [35]. The chosen central wavelength of  $\lambda_0 = 740$  nm is close to the 730-nm zero-dispersion wavelength of the PCF, in order to minimize the spectral broadening, which enables optimal interference at the 90:10 BS. The measured group-velocity dispersion of the PCF at 740 nm is  $-2$  ps<sup>2</sup>/km. The zero-dispersion wavelength of the PCF may be tailored by the fiber structure, making this approach applicable to a large range of wavelengths. The average optical power of the output state is 0.2 mW, which equates to 25 W of peak power. The amplitude squeezed light passes through a Thorlabs EO-AM-NR-C1 electro-optic modulator, which modulates polarization. A subsequent polarizing beam splitter translates the polarization modulation into a weak AM of depth  $\delta_m$ , and generates optical sidebands at distance  $\pm\Omega$  from the carrier frequency. The resulting state is measured with direct detection, by collecting all the light at photodiode PD1. We calibrate the shot-noise level using the balanced subtraction photocurrent of PD1 and PD2. The balanced amplified photodetector used is a Thorlabs PDB440A (-AC). The spectral photocurrent is analyzed with a Rohde & Schwarz FPC1000 spectrum analyzer.

### IV. EXPERIMENTAL RESULTS

The noise power spectra of amplitude-modulated squeezed light ( $-1.2$  dB) and antisqueezed light ( $2.7$  dB) produced by the setup are shown in Fig. 2(a). The RBW is  $B = 10$  kHz, which is considerably wider than the linewidth of the optical sidebands, measured to be  $< 1$  Hz. The frequency separation of trace points in Fig. 2(a) is smaller than the RBW since the trace is a result of multiple samples within each RBW interval. The electronic noise has been subtracted from each trace. This measurement demonstrates enhanced sensitivity detection of AM due to amplitude squeezing, as shown in [18].

From Eq. (9) we know that  $\text{Var}(\hat{\delta}_m)$  is proportional to  $\Phi$  and inversely proportional to  $\langle P \rangle$ . However, the profile of squeezing with optical power is such that change in power is negligible across the maximum observed squeezing range  $[-1.6, 2.7]$  dB in our setup, so here  $\text{Var}(\hat{\delta}_m)$  scales linearly with  $\Phi$ . By fitting measured  $\text{Var}(\hat{\delta}_m)$  to a line, we infer measured quantum precision enhancement using

$$Q(\hat{\delta}_m) = \frac{\text{Var}(\hat{\delta}_m)_{\text{QNL}}}{\text{Var}(\hat{\delta}_m)_{\Phi}}, \quad (11)$$

where  $\text{Var}(\hat{\delta}_m)_{\text{QNL}}$  and  $\text{Var}(\hat{\delta}_m)_{\Phi}$  are variances of estimates of  $\delta_m$  for coherent and squeezed light, respectively.

Figure 2(b) shows measured  $Q(\hat{\delta}_m)$  for a range of squeezing  $\Phi$  with fixed RBW  $B = 100$  kHz. The value of  $\delta_m$  has a small experimental drift, which varies between  $\delta_m = [0.8, 1.0] \times 10^{-4}$  over the duration of the measurements. Each sample of the spectral noise power corresponds to  $M \approx 34$ , due to the video bandwidth filter, and every measurement of  $\text{Var}(\hat{\delta}_m)_{\Phi}$  is taken from 50 samples of  $\hat{\delta}_m$ . Due to the high RBW, quantum noise limits the variance of  $\hat{\delta}_m$ , and the measurement saturates the optimal quantum bound  $Q_{\text{opt}}$  given by Eq. (10) (red curve). A precision enhancement of  $Q(\hat{\delta}_m) = 1.44 \pm 0.09$  is observed with  $-1.6$  dB of squeezing, in agreement with  $Q_{\text{opt}} = 1.45$ .

By repeating this for a range of  $B$  and a fixed  $-1.3$  dB of average squeezing, we plot in Fig. 2(c) the dependence of  $Q(\hat{\delta}_m)$  on RBW. The red curve is a theoretical fitting calculated using Eq. (8), with  $\text{Var}(\text{Re}[\mathcal{H}])$  as a fitting parameter, which gives  $\text{Var}(\text{Re}[\mathcal{H}]) = 7 \pm 1 \times 10^{-6}$ . We observe sub-QNL precision down to  $B = 100$  Hz. The maximum precision enhancement observed here is  $Q(\hat{\delta}_m) = 1.34 \pm 0.07$ , which again closely agrees with the the optimal  $Q_{\text{opt}} = 1.35$  for the average squeezing parameter of  $\Phi = 0.74$ . In Figs. 2(b) and 2(c), the error bars are derived from standard propagation of error calculations, with the data averaged over 236 variance measurements. Reducing optical loss to measure higher squeezing



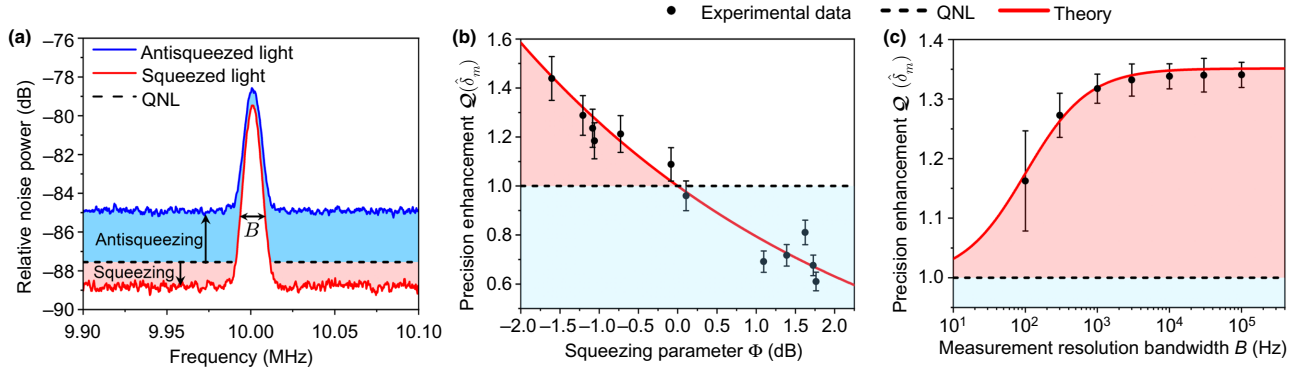


FIG. 2. Observing a precision enhancement in parameter estimation using amplitude squeezed light. In each panel, the black dashed line represents the QNL. (a) 10-MHz AM measured by direct detection. The red trace corresponds to  $-1.2$  dB of squeezing and the blue trace to  $2.7$  dB of antisqueezing. (b) Measured quantum precision enhancement of experimentally estimated  $\delta_m$ ,  $Q(\hat{\delta}_m)$ , for different squeezing  $\Phi$ . The red line corresponds to  $Q_{\text{opt}}$ . (c) Measured  $Q(\hat{\delta}_m)$  with varied RBW  $B$ , for an average  $-1.3$  dB of squeezing.

[9] enables greater enhancement in precision. Accounting for detection efficiency (we measure  $\eta_d = 0.84$ ) and coupling efficiency between the interferometer output and the detector ( $\eta_{\text{opt}} = 0.81$ ), we infer our maximum measured squeezing value of  $-1.6$  dB corresponds to  $-2.6$  dB of generated amplitude squeezing.

## V. CONCLUSION

We demonstrate quantum enhanced precision parameter estimation with bright squeezed amplitude light. We analyze the variance of the signal power in the presence of excess laser noise, and show that the degree of quantum precision enhancement is dictated by the amount of squeezing, the RBW, and the classical noise on the generated sidebands. This exemplifies that for measurements of high-power optical signals, sub-shot-noise sensitivity does not alone imply sub-shot-noise precision. The analysis is therefore essential in finding the conditions required for precision enhancement. We verify our model with experiment, reporting up to a 44% quantum enhancement in precision in the estimation of the modulation index, per detected photon. Our results can be directly transferred to other published state-of-the-art squeezed light sources (e.g., the source described in Ref. [37]). This general demonstration motivates applications in areas such as spectroscopy [38] and imaging [39], where precision may determine the performance of the measurement, which can be improved by using squeezed light. We use amplitude squeezed light of  $0.2$  mW average optical power ( $25$  W peak power) as a probe. This power is comparable to the photon dose required to induce a photophobic response in living cells [40], therefore indicating this technique's relevance to biological measurements.

Supporting data are available at the University of Bristol data repository [41].

## ACKNOWLEDGMENTS

We thank J. Mueller, P. Mosley, A. Politi, J. Rarity, N. Samantaray, W. Wadsworth, S. Wollmann, and W. Bowen for helpful discussions. This work is supported by QuantIC—the UK Quantum Technology Hub in Quantum Imaging (EPSRC EP/T00097X/1). G.S.A. is supported by the Quantum Engineering Centre for Doctoral Training (EPSRC EP/L015730/1). E.J.A. acknowledges fellowship support from EPSRC Doctoral Prize Fellowship (EP/R513179/1). J.C.F.M. acknowledges support from an EPSRC Quantum Technology Fellowship (EP/M024385/1) and European Research Council starting grant ERC-2018-STG 803665.

## APPENDIX A: CALCULATION OF THE SIGNAL-TO-NOISE RATIO

Here we derive the expected value of the electronic power  $p_\Omega$  in the  $\pm B/2$  frequency interval centered on the modulation frequency  $\Omega$ , generated by the current  $\hat{i}(t)$ . We may write  $p_\Omega$  as

$$p_\Omega = 2R|\hat{i}_\Omega|^2, \quad (\text{A1})$$

where  $R$  is the input resistance,  $\hat{i}_\Omega = \int^{\Omega} \hat{i}(\nu) d\nu$  is the photocurrent in the frequency bin centered on  $\Omega$ , using the notation  $\int^{\Omega} \equiv \int_{\Omega-B/2}^{\Omega+B/2}$ , and the factor of 2 comes from the integration over positive and negative frequencies. It is important to note that this differs from an often quoted definition of the power in a frequency band,  $p_\Omega = 2R \int^{\Omega} |\hat{i}(\nu)|^2 d\nu$  [1]. The reason for the definition used in Eq. (A1) is that measuring devices such as spectrum analyzers and oscilloscopes are fundamentally voltage detectors, and therefore the displayed power level is computed from the voltage measured in a given frequency bin. This means that the integration of the photocurrent density effectively occurs before taking the absolute square.

While the average value  $\langle p_\Omega \rangle$  does not significantly differ between these definitions,  $\text{Var}(p_\Omega)$  does. To keep the model consistent with the measurements obtained by our spectrum analyzer, we use Eq. (A1) as a definition for  $p_\Omega$ .

The amplitude of the optical field before modulation is applied may be written as  $\hat{A}_0(t) = [1 + \zeta(t)]\alpha_0 e^{i\theta} + \hat{a}(t)$ , where  $\theta$  is the phase of the classical field,  $\hat{a}(t)$  describes the quantum amplitude fluctuations, and  $\zeta(t)$  is a stochastic noise function that corresponds to the low-frequency classical noise of the laser. We assume a continuous-wave amplitude  $\alpha_0$  for simplicity. By making the assumption of large amplitude  $\alpha \gg 1$  and small modulation  $\Psi_m \ll 1$ , the amplitude  $\hat{A}(t)$  of the detected light after modulation may be written as

$$\begin{aligned} \hat{A}(t) &\approx [\Psi_0 + \Psi_m \cos(2\pi\Omega t)][1 + \zeta(t)]\alpha e^{i\theta} + \hat{a}(t) \\ &\equiv |\alpha(t)|e^{i\theta} + \hat{a}(t), \end{aligned} \quad (\text{A2})$$

where  $\Psi_0$  and  $\Psi_m$  are related to the modulation index by  $\Psi_0 = 1 - \delta_m/2$  and  $\Psi_m = \delta_m/2$ , and the detection efficiency  $\eta$  is modeled as an additional loss before detection, such that  $\alpha = \sqrt{\eta}\alpha_0$ . The effect of amplitude modulation on the quantum noise term has been neglected due to the small-modulation assumption. The current at time  $t$  may then be written as

$$\begin{aligned} \hat{i}(t) &= q \left[ \hat{A}(t)^\dagger \hat{A}(t) + n_e(t) \right] \\ &= q \left[ |\alpha(t)|^2 + \sqrt{2}|\alpha(t)|\hat{x}_\theta(t) + \hat{a}(t)^\dagger \hat{a}(t) + n_e(t) \right], \end{aligned} \quad (\text{A3})$$

where we have defined the quadrature operator  $\hat{x}_\theta(t) = (1/\sqrt{2})[\hat{a}(t)e^{-i\theta} + \hat{a}(t)^\dagger e^{i\theta}]$  and the electronic noise term

$n_e(t)$  corresponds to the number of electrons generated independently of the optical field. The component of the photocurrent at frequency  $\nu$  is then given by

$$\begin{aligned} \hat{i}(\nu) &= q \left[ I(\nu) + \sqrt{2} \int \alpha(\mu)\hat{x}_\theta(\nu - \mu)d\mu \right. \\ &\quad \left. + \int \hat{a}(-\mu)^\dagger \hat{a}(\nu - \mu)d\mu \right], \end{aligned} \quad (\text{A4})$$

where  $\int \equiv \int_{-\infty}^{\infty}$ , and we have defined the unitary Fourier transforms

$$I(\nu) = \int [|\alpha(t)|^2 + n_e(t)] e^{-2\pi i\nu t} dt \quad (\text{A5})$$

and

$$\hat{x}_\theta(\nu) = \int \hat{x}_\theta(t) e^{-2\pi i\nu t} dt = \frac{1}{\sqrt{2}} [\hat{a}(-\nu)^\dagger e^{i\theta} + \hat{a}(\nu) e^{-i\theta}]. \quad (\text{A6})$$

We also define  $\hat{a}(\nu)$  as the squeezed vacuum operator [42]

$$\hat{a}(\nu) = \hat{b}(\nu) \cosh r(\nu) - e^{2i\theta(\nu)} \hat{b}(-\nu)^\dagger \sinh r(\nu), \quad (\text{A7})$$

where  $\hat{b}(\nu)$  and  $\hat{b}(\nu)^\dagger$  are the bosonic creation and annihilation operators. The squeezing is defined such that  $r(\nu) = r$  and  $\theta(\nu) = \theta$  within the frequency bandwidth  $-\Lambda/2 \leq \nu \leq \Lambda/2$  (where  $\Lambda/2 > \Omega$ ) and  $r(\nu) = 0$  outside of this frequency range. The  $2\theta$  phase factor then orients the squeezing in the amplitude direction. By defining  $I_\Omega = \int^\Omega I(\nu) d\nu$  we can write  $p_\Omega$  as

$$\begin{aligned} p_\Omega &= 2q^2 R \left[ |I_\Omega|^2 + \sqrt{2}I_\Omega^* \int^\Omega \int \alpha(\mu)\hat{x}_\theta(\nu - \mu)d\mu d\nu + I_\Omega^* \int^\Omega \int \hat{a}(-\mu)^\dagger \hat{a}(\nu - \mu)d\mu d\nu \right. \\ &\quad + \sqrt{2}I_\Omega \int^\Omega \int \alpha(\mu)^* \hat{x}_\theta(\nu - \mu)^\dagger d\mu d\nu + 2 \int^\Omega \int^\Omega \int \alpha(\mu)^* \alpha(\bar{\mu}) \hat{x}_\theta(\nu - \mu)^\dagger \hat{x}_\theta(\bar{\nu} - \bar{\mu}) d\mu d\bar{\mu} d\nu d\bar{\nu} \\ &\quad + \sqrt{2} \int^\Omega \int^\Omega \int \alpha(\mu)^* \hat{x}_\theta(\nu - \mu)^\dagger \hat{a}(-\bar{\mu})^\dagger \hat{a}(\bar{\nu} - \bar{\mu}) d\mu d\bar{\mu} d\nu d\bar{\nu} \\ &\quad + I_\Omega \int^\Omega \int \hat{a}(\nu - \mu)^\dagger \hat{a}(-\mu) d\mu d\nu \\ &\quad + \sqrt{2} \int^\Omega \int^\Omega \int \alpha(\mu) \hat{a}(\nu - \bar{\mu})^\dagger \hat{a}(-\bar{\mu}) \hat{x}_\theta(\bar{\nu} - \mu) d\mu d\bar{\mu} d\nu d\bar{\nu} \\ &\quad \left. + \int^\Omega \int^\Omega \int \hat{a}(\nu - \mu)^\dagger \hat{a}(-\mu) \hat{a}(-\bar{\mu})^\dagger \hat{a}(\bar{\nu} - \bar{\mu}) d\mu d\bar{\mu} d\nu d\bar{\nu} \right], \end{aligned} \quad (\text{A8})$$

where  $(\bullet)^*$  denotes the complex conjugate. From Eq. (A2), we can find the frequency dependence of the classical field amplitude:

$$\alpha(\nu) = \int |\alpha(t)| e^{-2\pi i \nu t} = \alpha \left[ \Psi_0 [\delta(\nu) + h(\nu)] + \frac{\Psi_m}{2} [\delta(\nu - \Omega) + \delta(\nu + \Omega) + h(\nu - \Omega) + h(\nu + \Omega)] \right], \quad (\text{A9})$$

where  $h(\nu) = \int \zeta(t) e^{-2\pi i \nu t} dt$ , and since classical noise is only observed at low frequencies ( $\lesssim 2$  MHz), we can write for example  $h(\Omega) = 0$ . Equation (A2) allows us to define  $I(\nu)$  as

$$\begin{aligned} I(\nu) = & \alpha^2 \left[ \Psi_0^2 \left( \delta(\nu) + 2h(\nu) + \int h(\mu) h(\nu - \mu) d\mu \right) + \Psi_0 \Psi_m \left( \delta(\Omega - \nu) + \delta(\Omega + \nu) \right. \right. \\ & + 2h(\nu - \Omega) + 2h(\nu + \Omega) + \int h(\mu) h(\nu - \mu - \Omega) d\mu + \int h(\mu) h(\nu - \mu + \Omega) d\mu \left. \left. \right) \right. \\ & + \frac{\Psi_m^2}{4} \left( \delta(\nu - 2\Omega) + \delta(\nu + 2\Omega) + 2\delta(\nu) + 2h(\nu - 2\Omega) + 2h(\nu + 2\Omega) + 4h(\nu) \right. \\ & + \left. \int h(\mu) h(\nu - \mu - 2\Omega) d\mu + \int h(\mu) h(\nu - \mu + 2\Omega) d\mu + 2 \int h(\mu) h(\nu - \mu) d\mu \right) \left. \right] \\ & + n_e(\nu). \end{aligned} \quad (\text{A10})$$

We can then find the expectation  $\langle p_\Omega \rangle$  with respect to the random variables  $h(\nu)$ ,  $n_e(\nu)$ , and  $\hat{a}(\nu)$ . Since these variables are independent, the expectation value may be defined as  $\langle \bullet \rangle \equiv \langle \langle 0 | \bullet | 0 \rangle \rangle_{h(\nu), n_e(\nu)}$ . To calculate this, we first compute

$$\begin{aligned} |I_\Omega|^2 = & \Psi_0^2 \Psi_m^2 \alpha^4 \left[ 1 + 4 \int^\Omega \text{Re}[h(\nu - \Omega)] d\nu \right. \\ & + 2 \int^\Omega \int^\Omega \text{Re}[h(\mu) h(\nu - \mu - \Omega)] d\mu d\nu + 4 \left| \int^\Omega h(\nu - \Omega) d\nu \right|^2 \\ & + 4 \int^\Omega \int^\Omega \int^\Omega \text{Re}[h(\nu - \Omega)^* h(\mu) h(\bar{\nu} - \mu - \Omega)] d\mu d\nu d\bar{\nu} + \left| \int^\Omega \int^\Omega h(\mu) h(\nu - \mu - \Omega) d\mu d\nu \right|^2 \left. \right] \\ & + \Psi_0 \Psi_m \alpha^2 \left[ 2 \int^\Omega \text{Re}[n_e(\nu)] d\nu + 4 \int^\Omega \int^\Omega \text{Re}[h(\nu - \Omega)^* n_e(\bar{\nu})] d\nu d\bar{\nu} \right. \\ & + \left. 2 \int^\Omega \int^\Omega \int^\Omega \text{Re}[h(\mu)^* h(\nu - \mu - \Omega)^* n_e(\bar{\nu})] d\mu d\nu d\bar{\nu} \right] + \left| \int^\Omega n_e(\nu) d\nu \right|^2, \end{aligned} \quad (\text{A11})$$

where  $\text{Re}[\bullet]$  signifies the real part. Then, by evaluating the quantum part of the expectation value, we obtain the following result:

$$\begin{aligned} \langle p_\Omega \rangle = & 2q^2 R \left[ \langle |I_\Omega|^2 \rangle + \Phi \int^\Omega \int^\Omega \int^\Omega \langle \alpha(\mu)^* \alpha(\mu + \nu - \bar{\nu}) \rangle d\mu d\nu d\bar{\nu} + B\Lambda \left( \frac{\Phi^2}{8} + \frac{1}{8\Phi^2} - \frac{1}{4} \right) \right] \\ = & 2q^2 R \left[ \alpha^4 \left( \Psi_0^2 \Psi_m^2 + 2\Psi_0^2 \Psi_m^2 \int^\Omega \int^\Omega \langle \text{Re}[h(\mu) h(\nu - \mu - \Omega)] \rangle d\mu d\nu \right. \right. \\ & \left. \left. + 4\Psi_0^2 \Psi_m^2 \left\langle \left| \int^\Omega h(\nu - \Omega) d\nu \right|^2 \right\rangle \right) \right] \end{aligned}$$

$$\begin{aligned}
& + 4\Psi_0^2\Psi_m^2 \int^{\Omega} \int^{\Omega} \int (\text{Re}[h(v-\Omega)^*h(\mu)h(\bar{v}-\mu-\Omega)])d\mu dv d\bar{v} \\
& + \Psi_0^2\Psi_m^2 \left\langle \left| \int^{\Omega} \int h(\mu)h(v-\mu-\Omega)d\mu dv \right|^2 \right\rangle \\
& + \alpha^2 \left( \left( \Psi_0^2 + \frac{\Psi_m^2}{2} \right) \Phi B + \left( \Psi_0^2 + \frac{\Psi_m^2}{2} \right) \Phi \int^{\Omega} \int^{\Omega} \int \langle h(\mu)^*h(\mu+v-\bar{v}) \rangle d\mu dv d\bar{v} \right) \\
& + \left\langle \left| \int^{\Omega} n_e(v)dv \right|^2 \right\rangle + B\Lambda \left( \frac{\Phi^2}{8} + \frac{1}{8\Phi^2} - \frac{1}{4} \right), \tag{A12}
\end{aligned}$$

for the squeezing parameter  $\Phi = e^{-2r}$ . In Eq. (A12), we have neglected terms involving the expectation value of the product of an odd number of creation or annihilation operators, and terms outside the domain of  $h(v)$ . We have also used the fact that the expected amplitude of the classical noise terms  $\langle h(v) \rangle = \langle n_e(v) \rangle = 0$ , since the corresponding stochastic time-domain functions have a mean of zero. By observing that  $\alpha \gg 1$ ,  $\langle |\int h(v)dv| \rangle \ll 1$ , and  $\delta_m \ll 1$  for  $i_0 \approx q\alpha^2$ , we find

$$\langle p_{\Omega} \rangle \approx R \left( \frac{i_0^2 \delta_m^2}{2} + 2qi_0\Phi B + 2q^2 \left\langle \left| \int^{\Omega} n_e(v)dv \right|^2 \right\rangle \right). \tag{A13}$$

Similarly, at a small frequency interval  $\Delta f$  from  $\Omega$ , we find that the electronic powers of the optical noise floor and electronic noise floor are, respectively,

$$\begin{aligned}
\langle p_N \rangle & \approx R \left( 2qi_0\Phi B + 2q^2 \left\langle \left| \int^{\Omega} n_e(v)dv \right|^2 \right\rangle \right) \\
\text{and } \langle p_E \rangle & = R \left( 2q^2 \left\langle \left| \int^{\Omega} n_e(v)dv \right|^2 \right\rangle \right). \tag{A14}
\end{aligned}$$

We then find that the optical signal-to-noise ratio  $\delta_{\text{SNR}}$  may be expressed as

$$\delta_{\text{SNR}} = \frac{\langle p_{\Omega} \rangle - \langle p_N \rangle}{\langle p_N \rangle - \langle p_E \rangle} \approx \frac{i_0 \delta_m^2}{4q\Phi B}. \tag{A15}$$

## APPENDIX B: CALCULATION OF THE VARIANCE OF THE SIDEBAND POWER

In order to calculate the variance  $\text{Var}(p_{\Omega}) = \langle p_{\Omega}^2 \rangle - \langle p_{\Omega} \rangle^2$ , an expression for  $\langle p_{\Omega} \rangle^2$  may be evaluated directly from Eq. (A12). Here, we neglect quantum noise terms smaller than  $\mathcal{O}(n^3)$ , where  $n = \alpha^2$  is the number of detected photons. However, the variance calculation including all terms is provided in the Supplemental Material [43], which gives the same result. The result for  $\langle p_{\Omega} \rangle^2$  is

$$\begin{aligned}
\langle p_{\Omega} \rangle^2 & = 4q^4 R^2 \left[ \langle |I_{\Omega}|^2 \rangle^2 + (2\Psi_0^2 + \Psi_m^2) \langle |I_{\Omega}|^2 \rangle \alpha^2 \left( \Phi B \right. \right. \\
& \left. \left. + \Phi \int^{\Omega} \int^{\Omega} \int \langle h(\mu)^*h(\mu+v-\bar{v}) \rangle d\mu dv d\bar{v} \right) \right]. \tag{B1}
\end{aligned}$$



To find an expression for  $\langle p_\Omega^2 \rangle$ , we can again neglect terms where the expectation value of the quadrature operators vanishes, and terms smaller than  $\mathcal{O}(n^3)$ , giving

$$\begin{aligned} \langle p_\Omega^2 \rangle = & 4q^4 R^2 \left\langle |I_\Omega|^4 + 4|I_\Omega|^2 \int^\Omega \int^\Omega \int^\Omega \int^\Omega \alpha(\mu)^* \alpha(\bar{\mu}) \hat{x}_\theta(v - \mu)^\dagger \hat{x}_\theta(\bar{v} - \bar{\mu}) d\mu d\bar{\mu} dv d\bar{v} \right. \\ & + 2I_\Omega^{*2} \int^\Omega \int^\Omega \int^\Omega \int^\Omega \alpha(\mu) \alpha(\bar{\mu}) \hat{x}_\theta(v - \mu) \hat{x}_\theta(\bar{v} - \bar{\mu}) d\mu d\bar{\mu} dv d\bar{v} \\ & + 2I_\Omega^2 \int^\Omega \int^\Omega \int^\Omega \int^\Omega \alpha(\mu)^* \alpha(\bar{\mu})^* \hat{x}_\theta(v - \mu)^\dagger \hat{x}_\theta(\bar{v} - \bar{\mu})^\dagger d\mu d\bar{\mu} dv d\bar{v} \\ & \left. + 4|I_\Omega|^2 \int^\Omega \int^\Omega \int^\Omega \int^\Omega \alpha(\mu) \alpha(\bar{\mu})^* \hat{x}_\theta(v - \mu) \hat{x}_\theta(\bar{v} - \bar{\mu})^\dagger d\mu d\bar{\mu} dv d\bar{v} \right\rangle. \end{aligned} \tag{B2}$$

To explicitly evaluate  $\langle p_\Omega^2 \rangle$  in the following, we calculate the integrals in Eq. (B2) separately, using Eq. (A9) and the commutation relations of the Bose operators with the expectation value taken on the vacuum state. Terms 2–5 of Eq. (B2), respectively, give

$$\begin{aligned} & \left\langle 4|I_\Omega|^2 \int^\Omega \int^\Omega \int^\Omega \int^\Omega \alpha(\mu)^* \alpha(\bar{\mu}) \hat{x}_\theta(v - \mu)^\dagger \hat{x}_\theta(\bar{v} - \bar{\mu}) d\mu d\bar{\mu} dv d\bar{v} \right\rangle \\ & = (2\Psi_0^2 + \Psi_m^2) \alpha^2 \Phi \left( \langle |I_\Omega|^2 \rangle B + 2 \int^\Omega \int^\Omega \langle |I_\Omega|^2 \text{Re}[h(v - \bar{v})] \rangle dv d\bar{v} \right. \\ & \quad \left. + \int^\Omega \int^\Omega \int^\Omega \langle |I_\Omega|^2 h(\mu)^* h(\mu + v - \bar{v}) \rangle d\mu dv d\bar{v} \right), \end{aligned} \tag{B3}$$

$$\begin{aligned} & \left\langle 2I_\Omega^{*2} \int^\Omega \int^\Omega \int^\Omega \int^\Omega \alpha(\mu) \alpha(\bar{\mu}) \hat{x}_\theta(v - \mu) \hat{x}_\theta(\bar{v} - \bar{\mu}) d\mu d\bar{\mu} dv d\bar{v} \right\rangle \\ & = \frac{\Psi_m^2}{4} \alpha^2 \Phi \left( \langle I_\Omega^{*2} \rangle B + 2 \int^\Omega \int^\Omega \langle I_\Omega^{*2} h(v + \bar{v} - 2\Omega) \rangle dv d\bar{v} \right. \\ & \quad \left. + \int^\Omega \int^\Omega \int^\Omega \langle I_\Omega^{*2} h(\mu - \Omega) h(v + \bar{v} - \mu - \Omega) \rangle d\mu dv d\bar{v} \right), \end{aligned} \tag{B4}$$

$$\begin{aligned} & \left\langle 2I_\Omega^2 \int^\Omega \int^\Omega \int^\Omega \int^\Omega \alpha(\mu)^* \alpha(\bar{\mu})^* \hat{x}_\theta(v - \mu)^\dagger \hat{x}_\theta(\bar{v} - \bar{\mu})^\dagger d\mu d\bar{\mu} dv d\bar{v} \right\rangle \\ & = \frac{\Psi_m^2}{4} \alpha^2 \Phi \left( \langle I_\Omega^2 \rangle B + 2 \int^\Omega \int^\Omega \langle I_\Omega^2 h(v + \bar{v} - 2\Omega)^* \rangle dv d\bar{v} \right. \\ & \quad \left. + \int^\Omega \int^\Omega \int^\Omega \langle I_\Omega^2 h(\mu - \Omega)^* h(v + \bar{v} - \mu - \Omega)^* \rangle d\mu dv d\bar{v} \right), \end{aligned} \tag{B5}$$

and

$$\begin{aligned} & \left\langle 4|I_\Omega|^2 \int^\Omega \int^\Omega \int^\Omega \int^\Omega \alpha(\mu) \alpha(\bar{\mu})^* \hat{x}_\theta(v - \mu) \hat{x}_\theta(\bar{v} - \bar{\mu})^\dagger d\mu d\bar{\mu} dv d\bar{v} \right\rangle \\ & = (2\Psi_0^2 + \Psi_m^2) \alpha^2 \Phi \left( \langle |I_\Omega|^2 \rangle B + 2 \int^\Omega \int^\Omega \langle |I_\Omega|^2 \text{Re}[h(v - \bar{v})] \rangle dv d\bar{v} \right. \\ & \quad \left. + \int^\Omega \int^\Omega \int^\Omega \langle |I_\Omega|^2 h(\mu)^* h(\mu + v - \bar{v}) \rangle d\mu dv d\bar{v} \right). \end{aligned} \tag{B6}$$

Combining these terms for Eq. (B2), we obtain

$$\begin{aligned}
\langle p_\Omega^2 \rangle = & 4q^4 R^2 \left[ \langle |I_\Omega|^4 \rangle + (4\Psi_0^2 + 2\Psi_m^2)\alpha^2 \Phi \left( \langle |I_\Omega|^2 \rangle B + 2 \int^\Omega \int^\Omega \langle |I_\Omega|^2 \text{Re}[h(\nu - \bar{\nu})] \rangle d\nu d\bar{\nu} \right. \right. \\
& + \left. \int^\Omega \int^\Omega \int \langle |I_\Omega|^2 h(\mu)^* h(\mu + \nu - \bar{\nu}) \rangle d\mu d\nu d\bar{\nu} \right) \\
& + \frac{\Psi_m^2}{2} \alpha^2 \Phi \left( \langle \text{Re}[I_\Omega^{*2}] \rangle B + 2 \int^\Omega \int^\Omega \langle \text{Re}[I_\Omega^{*2} h(\nu + \bar{\nu} - 2\Omega)] \rangle d\nu d\bar{\nu} \right. \\
& \left. \left. + \int^\Omega \int^\Omega \int \langle \text{Re}[I_\Omega^{*2} h(\mu - \Omega) h(\nu + \bar{\nu} - \mu - \Omega)] \rangle d\mu d\nu d\bar{\nu} \right) \right]. \tag{B7}
\end{aligned}$$

In the expression for  $\text{Var}(p_\Omega) = \langle p_\Omega^2 \rangle - \langle p_\Omega \rangle^2$ , there is significant cancellation between  $\langle p_\Omega^2 \rangle$  and  $\langle p_\Omega \rangle^2$ , and by taking the leading remaining terms we find that

$$\begin{aligned}
\text{Var}(p_\Omega) = & \langle p_\Omega^2 \rangle - \langle p_\Omega \rangle^2 \approx 4q^4 R^2 \left[ \langle |I_\Omega|^4 \rangle - \langle |I_\Omega|^2 \rangle^2 + 2\langle |I_\Omega|^2 \rangle \Psi_0^2 \alpha^2 \Phi B \right] \\
& \approx 4q^4 R^2 \left[ 16\Psi_0^4 \Psi_m^4 \alpha^8 \int^\Omega \int^\Omega \langle \text{Re}[h(\nu - \Omega)] \text{Re}[h(\bar{\nu} - \Omega)] \rangle d\nu d\bar{\nu} \right. \\
& \left. + 4\Psi_0^2 \Psi_m^2 \alpha^4 \int^\Omega \int^\Omega \langle \text{Re}[n_e(\nu)] \text{Re}[n_e(\bar{\nu})] \rangle d\nu d\bar{\nu} + 2\Phi B \Psi_0^4 \Psi_m^2 \alpha^6 \right]. \tag{B8}
\end{aligned}$$

By associating  $\mathcal{H} = \int^\Omega h(\nu - \Omega) d\nu = \int_{-B/2}^{B/2} h(\nu) d\nu$  as the relative amplitude of the classical optical noise in the dc component,  $\mathcal{N} = \int^\Omega n_e(\nu) d\nu$  as the amplitude of the electronic noise in the  $\pm B/2$  frequency interval around  $\Omega$ , and substituting  $\Psi_0 \approx 1$ ,  $\Psi_m = \delta_m/2$ , and  $i_0 \approx q\eta\alpha_0^2$ , we find that for  $M$  spectral averages,

$$\text{Var}(p_\Omega) \approx \frac{R^2}{M} \left[ 2q\delta_m^2 i_0^3 \Phi B + 4\delta_m^4 i_0^4 \text{Var}(\text{Re}[\mathcal{H}]) + 4q^2 \delta_m^2 i_0^2 \text{Var}(\text{Re}[\mathcal{N}]) \right]. \tag{B9}$$

From Eq. (B9), an improvement in precision beyond the quantum noise limit may be obtained in the case that squeezing ( $\Phi < 1$ ) provides a significant reduction in  $\text{Var}(p_\Omega)$ .

[1] H. A. Bachor and T. C. Ralph, *A Guide to Experiments in Quantum Optics* (Weinheim: Wiley-VCH, Weinheim, 2004), Vol. 1.  
[2] B. L. Higgins, D. W. Berry, S. D. Bartlett, H. M. Wiseman, and G. J. Pryde, Entanglement-free Heisenberg-limited phase estimation, *Nat.* **450**, 393 (2007).  
[3] P. M. Birchall, J. L. O'Brien, J. C. F. Matthews, and H. Cable, Quantum-classical boundary for precision optical phase estimation, *Phys. Rev. A* **96**, 062109 (2017).  
[4] E. J. Allen, J. Sabines-Chesterking, A. R. McMillan, S. K. Joshi, P. S. Turner, and J. C. F. Matthews, Approaching the quantum limit of precision in absorbance estimation using classical resources, *Phys. Rev. Res.* **2**, 033243 (2020).  
[5] R. Cole, Live-cell imaging: The cell's perspective, *Cell Adh. Migr.* **8**, 452 (2014).  
[6] M. Xiao, L.-A. Wu, and H. J. Kimble, Precision Measurement beyond the Shot-Noise Limit, *Phys. Rev. Lett.* **59**, 278 (1987).  
[7] M. A. Taylor, J. Janousek, V. Daria, J. Knittel, B. Hage, H. A. Bachor, and W. P. Bowen, Biological measurement beyond the quantum limit, *Nat. Photonics* **7**, 229 (2013).

[8] C. Gardiner and P. Zoller, *Quantum Noise: A Handbook of Markovian and Non-Markovian Quantum Stochastic Methods with Applications to Quantum Optics* (Springer Science & Business Media, Berlin, 2004), Vol. 56.  
[9] H. Vahlbruch, M. Mehmet, K. Danzmann, and R. Schnabel, Detection of 15 dB Squeezed States of Light and Their Application for the Absolute Calibration of Photoelectric Quantum Efficiency, *Phys. Rev. Lett.* **117**, 110801 (2016).  
[10] U. L. Andersen, T. Gehring, C. Marquardt, and G. Leuchs, 30 years of squeezed light generation, *Phys. Scr.* **91**, 053001 (2016).  
[11] M. Zwiernik, C. A. Pérez-Delgado, and P. Kok, General Optimality of the Heisenberg Limit for Quantum Metrology, *Phys. Rev. Lett.* **105**, 180402 (2010).  
[12] J. Minkoff, *Signal Processing Fundamentals and Applications for Communications and Sensing Systems* (Artech House, Boston, 2002).  
[13] S. Slussarenko, M. M. Weston, H. M. Chrzanowski, L. K. Shalm, V. B. Verma, S. W. Nam, and G. J. Pryde, Unconditional violation of the shot-noise limit in photonic quantum metrology, *Nat. Photonics* **11**, 700 (2017).

- [14] J. Sabines-Chesterking, R. Whittaker, S. K. Joshi, P. M. Birchall, P. A. Moreau, A. McMillan, H. V. Cable, J. L. O'Brien, J. G. Rarity, and J. C. F. Matthews, Sub-Shot-Noise Transmission Measurement Enabled by Active Feed-Forward of Heralded Single Photons, *Phys. Rev. Appl.* **8**, 014016 (2017).
- [15] G. Brida, M. Genovese, and I. R. Berchera, Experimental realization of sub-shot-noise quantum imaging, *Nat. Photonics* **4**, 227 (2010).
- [16] A. A. Berni, T. Gehring, B. M. Nielsen, V. Händchen, M. G. Paris, and U. L. Andersen, Ab initio quantum-enhanced optical phase estimation using real-time feedback control, *Nat. Photonics* **9**, 577 (2015).
- [17] H. Yonezawa, D. Nakane, T. A. Wheatley, K. Iwasawa, S. Takeda, H. Arai, K. Ohki, K. Tsumura, D. W. Berry, and T. C. Ralph *et al.*, Quantum-enhanced optical-phase tracking, *Science* **337**, 1514 (2012).
- [18] M. Xiao, L.-A. Wu, and H. J. Kimble, Detection of amplitude modulation with squeezed light for sensitivity beyond the shot-noise limit, *Opt. Lett.* **13**, 476 (1988).
- [19] P. Grangier, R. E. Slusher, B. Yurke, and A. LaPorta, Squeezed-Light-Enhanced Polarization Interferometer, *Phys. Rev. Lett.* **59**, 2153 (1987).
- [20] E. S. Polzik, J. Carri, and H. J. Kimble, Spectroscopy with Squeezed Light, *Phys. Rev. Lett.* **68**, 3020 (1992).
- [21] S. Kasapi, S. Lathi, and Y. Yamamoto, Amplitude-squeezed, frequency-modulated, tunable, diode-laser-based source for sub-shot-noise FM spectroscopy, *Opt. Lett.* **22**, 478 (1997).
- [22] Y. Q. Li, P. Lynam, M. Xiao, and P. J. Edwards, Sub-Shot-Noise Laser Doppler Anemometry with Amplitude-Squeezed Light, *Phys. Rev. Lett.* **78**, 3105 (1997).
- [23] J. L. Sørensen, J. Hald, and E. S. Polzik, Quantum Noise of an Atomic Spin Polarization Measurement, *Phys. Rev. Lett.* **80**, 3487 (1998).
- [24] F. Wolfgramm, A. Cere, F. A. Beduini, A. Predojević, M. Koschorreck, and M. W. Mitchell, Squeezed-Light Optical Magnetometry, *Phys. Rev. Lett.* **105**, 053601 (2010).
- [25] R. C. Pooser and B. Lawrie, Ultrasensitive measurement of microcantilever displacement below the shot-noise limit, *Optica* **2**, 393 (2015).
- [26] M. E. Tse, H. Yu, N. Kijbunchoo, A. Fernandez-Galiana, P. Dupej, L. Barsotti, C. D. Blair, D. D. Brown, S. E. Dwyer, and A. Effler *et al.*, Quantum-Enhanced Advanced LIGO Detectors in the era of Gravitational-Wave Astronomy, *Phys. Rev. Lett.* **123**, 231107 (2019).
- [27] F. Acernese, M. Agathos, L. Aiello, A. Allocca, A. Amato, S. Ansoldi, S. Antier, M. Arène, N. Arnaud, and S. Ascenzi *et al.*, Increasing the Astrophysical Reach of the Advanced Virgo Detector via the Application of Squeezed Vacuum States of Light, *Phys. Rev. Lett.* **123**, 231108 (2019).
- [28] R. B. de Andrade, H. Kerdoncuff, K. Berg-Sørensen, T. Gehring, M. Lassen, and U. L. Andersen, Quantum-enhanced continuous-wave stimulated Raman scattering spectroscopy, *Optica* **7**, 470 (2020).
- [29] G. T. Garces, H. M. Chrzanowski, S. Daryanoosh, V. Thiel, A. L. Marchant, R. B. Patel, P. C. Humphreys, A. Datta, and I. A. Walmsley, Quantum-enhanced stimulated emission detection for label-free microscopy, *Appl. Phys. Lett.* **117**, 024002 (2020).
- [30] C. A. Casacio, L. S. Madsen, A. Terrason, M. Waleed, K. Barnscheidt, B. Hage, M. A. Taylor, and W. P. Bowen, Quantum-enhanced nonlinear microscopy, *Nat.* **594**, 201 (2021).
- [31] D. Krylov and K. Bergman, Amplitude-squeezed solitons from an asymmetric fiber interferometer, *Opt. Lett.* **23**, 1390 (1998).
- [32] O. Svelto and D. C. Hanna, *Principles of Lasers* (Springer, New York, 1998), Vol. 4.
- [33] O. Pinel, P. Jian, N. Treps, C. Fabre, and D. Braun, Quantum parameter estimation using general single-mode Gaussian states, *Phys. Rev. A* **88**, 040102(R) (2013).
- [34] E. L. Lehmann and G. Casella, *Theory of Point Estimation* (Springer Science & Business Media, New York, 2006).
- [35] S. Schmitt, J. Ficker, M. Wolff, F. König, A. Sizmann, and G. Leuchs, Photon-Number Squeezed Solitons from an Asymmetric Fiber-Optic Sagnac Interferometer, *Phys. Rev. Lett.* **81**, 2446 (1998).
- [36] O. Alibart, J. Fulconis, G. K. L. Wong, S. G. Murdoch, W. J. Wadsworth, and J. G. Rarity, Photon pair generation using four-wave mixing in a microstructured fibre: Theory versus experiment, *New J. Phys.* **8**, 67 (2006).
- [37] K. Hirose, H. Furumochi, A. Tada, F. Kannari, M. Takeoka, and M. Sasaki, Photon Number Squeezing of Ultrabroadband Laser Pulses Generated by Microstructure Fibers, *Phys. Rev. Lett.* **94**, 203601 (2005).
- [38] R. Whittaker, C. Erven, A. Neville, M. Berry, J. L. O'Brien, H. Cable, and J. C. F. Matthews, Absorption spectroscopy at the ultimate quantum limit from single-photon states, *New J. Phys.* **19**, 023013 (2017).
- [39] J. Sabines-Chesterking, A. R. McMillan, P. A. Moreau, S. K. Joshi, S. Knauer, E. Johnston, J. G. Rarity, and J. C. F. Matthews, Twin-beam sub-shot-noise raster-scanning microscope, *Opt. Express* **27**, 30810 (2019).
- [40] P. Berthold, S. P. Tsunoda, O. P. Ernst, W. Mages, D. Gradmann, and P. Hegemann, Channelrhodopsin-1 initiates phototaxis and photophobic responses in chlamydomonas by immediate light-induced depolarization, *Plant Cell* **20**, 1665 (2008).
- [41] G. S. Atkinson, E. J. Allen, G. Ferranti, A. R. McMillan, and J. C. F. Matthews, Data for: "Quantum Enhanced Precision Estimation of Transmission with Bright Squeezed Light," University of Bristol, <https://doi.org/10.5523/bris.2g0fu4uyv5tf28qglaf23b2ti> (2021).
- [42] R. Loudon, *The Quantum Theory of Light* (OUP Oxford, Oxford, 2000).
- [43] See Supplemental Material at <http://link.aps.org/supplemental/10.1103/PhysRevApplied.16.044031> for the full calculation of the variance of the sideband power, including all photon number terms, which verifies the result of Eq. (B8).